# Understanding the ferromagnetic insulating state in Cr-doped $VO_2$: Density functional and tight binding calculations

Shishir Kumar Pandey,* Abhinav Kumar,* Sagar Sarkar, and Priya Mahadevan†
*Department of Condensed Matter Physics and Material Science, S. N. Bose National Center for Basic Sciences, 700106 Kolkata, India*

(Received 1 August 2019; revised 5 July 2021; accepted 16 August 2021; published 8 September 2021)

Experimentally, Cr doping in the rutile phase of $VO_2$ is found to stabilize a charge-ordered ferromagnetic insulating state in the doping range of 10% to 20%. In this work, we investigate its origin at 12.5% Cr doping using a combination of *ab initio* electronic structure calculations as well as microscopic modeling. Our calculations are found to reproduce the ferromagnetic insulating state as well as a charge ordering at the V and Cr sites. The mapping of the *ab initio* band structure onto a tight binding Hamiltonian allows one to calculate the energy gain from different exchange pathways. This gain is quantified in this work, and the role of charge ordering in stabilizing a ferromagnetic insulating state is understood.

DOI: 10.1103/PhysRevB.104.125110

## I. INTRODUCTION

Among the magnetic systems that one encounters, an empirical rule has emerged, which is that ferromagnetism is accompanied by a metallic ground state while antiferromagnetism is found in members that are insulating. The ones that break these empirical trends are the most interesting members as they would require a mechanism beyond the conventionally accepted theories to explain the origin of the magnetic state. Even from a technological standpoint ferromagnetic insulators are interesting [1,2] as information transfer can take place through spin waves, without charge displacement or eddy current losses. There have been several examples discovered recently which include the layered materials like $CrI_3$ and $VI_3$ [3,4] as well as a three-dimensional oxide $Sr_3OsO_6$ with a high ordering temperature [5]. The recently discovered layered van der Waals ferromagnet $Cr_2Ge_2Te_6$ is also found to be insulating [6]. However, the mechanism here as in several other compounds such as $CdCr_2S_4$ is 90° superexchange between the Cr atoms via the S atom [7]. This allows a ferromagnetic exchange pathway even in insulators. Ferromagnetic insulators are also found among the double perovskites of the form $A_2BB'O_6$. Here, the presence of different atoms at the $B$ and $B'$ sites, where the $B'$ site is usually nonmagnetic, leads to a superexchange pathway through the unoccupied states on the $B'$ atom that is operational even in an insulator. Even when the $B'$ site is magnetic, we have few examples of ferromagnetic insulators as found in $Bi_2NiMnO_6$ and $La_2NiMnO_6$ for instance [8,9]. The highly distorted perovskite oxide $YTiO_3$ was found to have a ferromagnetic ground state because of orbital ordering at the Ti site, which also explained the insulating character of the ground state [10]. There have been other examples found among the undoped oxides such as strained films of $LaCoO_3$, though the mechanism has not been clarified there [11]. The doped manganites [12] as well as the hollandites $K_2Cr_8O_{16}$ have an unusual ground state where charge ordering is found to co-exist with a ferromagnetic insulating state [13]. In Ref. [14] it was speculated that the charge ordering led to the presence of a superexchange pathway that could stabilize a ferromagnetic insulator. The present study allows us to examine the role played by charge ordering quantitatively.

While $V_{1-x}Cr_xO_2$ [15–17] in its monoclinic phase has been extensively studied for its metal-insulator transitions, the more recent stabilization of the rutile phase in Cr-doped $VO_2$ [18,19] led to the observation of a ferromagnetic insulating state. In this work, we examine the origin of this unusual ground state. The parent compounds $VO_2$ [20–23] and $CrO_2$ [24–27] are examples of an antiferromagnetic insulator (though in a different polymorph) and ferromagnetic metal, respectively. However, experiments have found that for Cr doping percentage from 10% to 20% in the rutile phase of $VO_2$, the system is found to become a ferromagnetic insulator [19]. X-ray absorption spectroscopy which, apart from being atom specific is also sensitive to the valence state, reveals the presence of $Cr^{+3}$-$V^{+5}$ pairs [19]. The question that follows is why do such charge states get stabilized and do they have a role in the unusual ferromagnetic insulating state found at this doping concentration.

V atoms have a valence state of +4 in $VO_2$, with the $d$ electrons on V having an electronic configuration of $d^1$. An isovalent substitution of V with Cr should result in a configuration of $d^2$ at the Cr sites. As the fully doped end member $CrO_2$ is metallic, one expects a metallic ground state to be favored above a critical doping concentration. While the transport properties of these systems have not been studied, x-ray absorption spectroscopy results which are sensitive to the valence state of the transition metal atoms reveal the presence of $V^{+5}$ as well as $Cr^{+3}$ species, in addition to $V^{+4}$ at 18% doping of Cr [19]. These results are suggestive of an insulating ground state being favored, as otherwise the free carriers present

*These authors contributed equally to this work.
†priya.mahadevan@gmail.com

 ©2021 American Physical Society

would result in all the V atoms having the same oxidation state.

In this work we have doped Cr into the experimentally observed rutile phase of $VO_2$ for doping concentrations of 12.5% and 25% and examined the ensuing electronic and magnetic ground states. A ferromagnetic insulating state is found at 12.5% which is consistent with the dopant range in experiments where it has been seen. The doped Cr atoms are found to be in the +3 valence state instead of +4 which is expected for an isovalent substitution. This is achieved by the transfer of an electron from one of the neighboring V sites, rendering the latter with a valency of +5. While the distortion of the Cr-O and V-O bond lengths involves a large component of strain energy to stabilize the unusual valencies of $Cr^{+3}$ and $V^{+5}$, the large Hund's intra-atomic exchange on Cr favoring a $d^3$ configuration as well as the attractive Coulomb interactions between $Cr^{+3}$-$V^{+5}$ ions help in stabilizing it. The charge ordering of $Cr^{+3}$-$V^{+5}$ ions also facilitates hopping if the spins are aligned ferromagnetically and is reminiscent of a "frozen-in" double-exchange configuration. We carry out a mapping of the *ab initio* band structure onto a tight binding model for the ferromagnetic case as well as the closest lying antiferromagnetic state at 12.5% doping. Within the model we determine the energy gain from the $Cr^{+3}$-$V^{+5}$ pathway as well as $Cr^{+3}$-$V^{+4}$ pathway and show for the first time how charge ordering can stabilize a ferromagnetic insulating state. This mechanism has to compete with other pathways present.

At 25% doping, the complexity of the possible competing magnetic ground states increases. This is because while the V atoms would prefer an antiferromagnetic ordering among themselves, the relative spin alignment of spins between Cr and V atoms depends on the separation between the Cr atoms. The half-filled $t_{2g}$ bands at the $Cr^{3+}$ site would like to be antiferromagnetic, while the pathway through $V^{5+}$ would favor a ferromagnetic ground state. Examining the lowest energy configuration here, we find it to be again a ferromagnetic insulator.

## II. METHODOLOGY

In order to calculate the electronic structure of Cr-doped $VO_2$, we have performed first-principles density functional theory based calculations using the Vienna *ab initio* simulation package [28]. We have used projected augmented wave [29] potentials for each atom. These include the semicore $p$ states on the V atom. We have used a gamma-centered $k$ mesh of $6 \times 6 \times 8$ for the 24-atom unit cell considered, which has been appropriately scaled for the larger supercell sizes considered. A plane wave cutoff of 875 eV was used in the calculations. The generalized gradient approximation (GGA) [30] was used for the exchange-correlation functional and electron-electron interactions were considered by including a Hubbard $U$ within the GGA + $U$ formalism [31]. One finds a variation of the $U$ from 2 to 4 eV for V and Cr in the literature [32–34]. This prompted us to explore variations of $U$ in this range, the details of which are given later in the paper. Having explored that the results are robust against variations in $U$, the rest of the discussion in the paper uses a $U$ of 2.5 eV on V atoms and a $U$ of 3 eV on the Cr atoms.

The total energy was calculated self-consistently till the energy difference between successive steps was better than $10^{-5}$ eV. The total energy of the ferromagnetic configuration was compared with the energy of other antiferromagnetic configurations within the 8-V-atom $\sqrt{2}\mathbf{a} \times \sqrt{2}\mathbf{b} \times 2\mathbf{c}$ supercell constructed using the experimental lattice parameters of $VO_2$ as the starting parameters, where $\mathbf{a} = \mathbf{b} = 6.441$ Å and $\mathbf{c} = 5.700$ Å [35]. We further optimized both the lattice parameters as well as the internal coordinates of the crystal. After optimization we found that **a** and **b** were slightly (approximately 0.6%–0.7%) underestimated while **c** was overestimated by 4.4% from its initial value (please see Table S1 of the Supplemental Material [36] for more details). As these results correspond to the specific case where we have $Cr^{+3}$-$V^{+5}$ pairs arranged alternately in the $c$ direction, we explored a larger unit cell $\sqrt{2}\mathbf{a} \times \sqrt{2}\mathbf{b} \times 4\mathbf{c}$ in which we doped pairs of Cr atoms. All distinct locations for the pair of Cr atoms were explored.

In order to understand the results further we have mapped the *ab initio* band structure onto a tight binding model using maximally localized Wannier functions for the radial part of the wave functions using the WANNIER90-VASP interface [37,38] implemented within VASP. The mapping was done for the 12.5% doping concentration which had 1 Cr atom in the unit cell and was done for both the ferromagnetic as well as the closest lying antiferromagnetic state. The basis we considered for the tight binding model included all five $d$ orbitals on Cr and V atoms as well as the three $p$ orbitals on oxygen atoms. A sufficiently large energy window spanning from −7.8 eV below $E_f$ to 4.2 eV above it was chosen to accommodate all the 88 Wannier functions of our basis. The spreads of each of the Wannier functions are given in the bottom part of Table S1 of the Supplemental Material [36], with the largest being found to be 0.547, 0.611, and 0.716 $Å^2$ for Cr and V $d$ and O $p$ orbitals, respectively. Consequently one can say that the Wannier functions are sufficiently localized and representative of the atomic-like orbitals. The mapping then allows us to extract the on-site energies as well as the hopping interaction strengths. Our band structure in the Wannier basis provides a very good description of the *ab initio* band structure. In Fig. S1 [36] we show the comparison when we retain interactions up to just 3.4 Å and see that retaining interactions till here provides us with a reasonable description of the electronic structure. As we now have the complete Hamiltonian, we switch off certain hopping pathways and determine the band energy, computed as the sum of the occupied eigenvalues, within the tight binding model. This allows us to determine the contribution from various exchange pathways in each magnetic configuration.

## III. RESULTS AND DISCUSSION

In order to understand the electronic and magnetic properties of $V_{1-x}Cr_xO_2$, we consider a supercell of $VO_2$ which has eight V atoms in it, shown in the left panel of Fig. 1. Each unit cell has four V chains running in the $c$ direction. This is also the direction in which the distance between neighboring V atoms is the shortest and is equal to 2.94 Å in the undoped case. The other neighboring V-V bond lengths are equal to 3.52 Å. In order to explore the modifications in the electronic

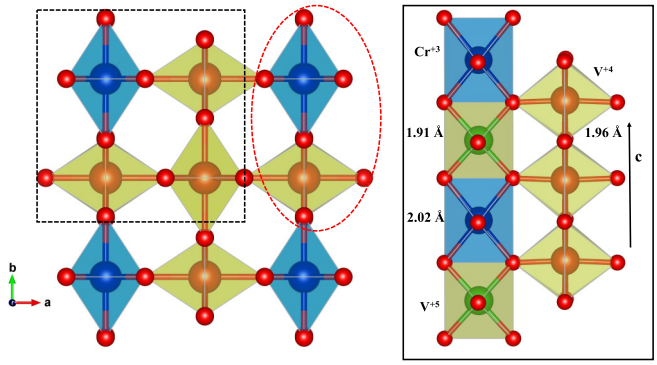



FIG. 1. The $\sqrt{2}\mathbf{a} \times \sqrt{2}\mathbf{a} \times 2\mathbf{c}$ supercell has been shown on the left while the formation of $Cr^{+3}$-$V^{+5}$ chains as well as the bond lengths have been shown in the right for 12.5% Cr doped in $VO_2$ (24-atom supercell). The blue and green balls represent $Cr^{+3}$ and $V^{+5}$ while $V^{+4}$ ions are represented by the orange balls. Dashed black line square box shows the rutile unit cell of $VO_2$ used to make the supercell considered in our study. Dashed red oval box shows arrangement of $Cr^{+3}$ -$V^{+4}$ chains along *b* direction.

structure at 12.5% doping, one V atom in this unit cell was replaced by a Cr atom. Displacing the atoms and minimizing their total energy, we found that the V-V distances are now modified and become 2.98 Å along the *c* direction, while the other V-V bond lengths are 3.52/3.53 Å. In order to find the ground state magnetic configuration, we examined the ferromagnetic as well as the antiferromagnetic configurations shown in Fig. 2.

In the antiferromagnetic configuration labeled AFM1, the coupling between the atoms in a chain is ferromagnetic. The neighboring chains are however coupled antiferromagnetically. The other antiferromagnetic configuration that was explored had the V atoms coupled antiferromagnetically along the chain, while they were ferromagnetic between nearest-neighbor chains. This was labeled AFM2. The unit cell parameters were optimized for each of the magnetic configurations considered. They did not show very large changes between the different configurations. The total energies determined for the ferromagnetic as well as various antiferromagnetic configurations are listed in Table I. The ferromagnetic configuration is found to be more stable than the closest antiferromagnetic configuration AFM1 by 100 meV

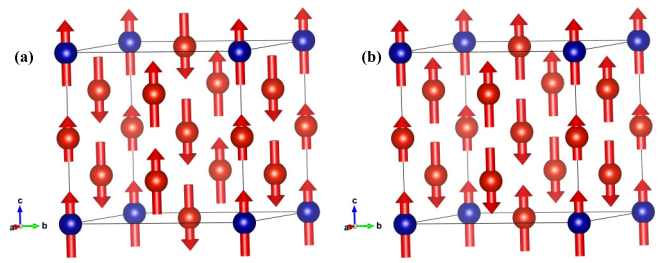



FIG. 2. (a) AFM1 and (b) AFM2 magnetic configurations for 12.5% Cr doping case. Blue balls are Cr atoms and red ones are V. Length of the arrow represents the corresponding magnitude of magnetic moments. Small red arrow corresponds to $V^{+5}$ ions with a tiny magnetic moment of 0.06 $\mu_B$.

TABLE I. Relative energies of different antiferromagnetic magnetic configurations per supercell (24 atoms/8 formula units) with respect to ferromagnetic configuration for 12.5% doping of Cr in rutile $VO_2$. Net magnetic moment (MM) is also given for each case.

| | Energy (eV) | MM ($\mu_B$) |
|---|---|---|
| FM | 0.0 | 9 |
| AFM1 | 0.1 | 1.0 |
| AFM2 | 0.12 | 3.0 |

per supercell. As we have a doped Cr atom which carries a different moment than the V atoms, we find a net moment for each of the antiferromagnetic configurations probed and this has been indicated in Table I. While the experimental ground state has not been examined at this composition, it has been found to be a ferromagnetic insulator at 10%, 18%, and 20%. The presence of a ferromagnetic insulating state seems unusual, so we examine the density of states at 12.5% where we already found a ferromagnetic ground state to be stabilized to see whether one finds an insulating state also.

The atom, angular momentum, and spin-projected density of states are shown for two distinct V atoms that we find in the unit cell as well as the Cr atom. The system is found to be insulating. As each transition metal atom is surrounded by six oxygens, the *d* orbitals at each transition metal site split into triply degenerate $t_{2g}$ orbitals at lower energies and doubly degenerate $e_g$ orbitals at higher energies. Examining the Cr *d* density of states shown in Fig. 3, one finds that the minority spin states lie beyond 3 eV above the Fermi level and are empty. The majority spin $t_{2g}$ states are however found to be occupied while the $e_g$ counterparts are found to be empty. An isovalent substitution of V by Cr would imply a valence state of +4 on Cr. However, we find the electron configuration of $t_{2g\uparrow}^3$ on Cr, implying a valence of +3. One of the V atoms has none of the *d* orbitals occupied and hence can be associated with a $d^0$ configuration. We identify a valence of +5 with this

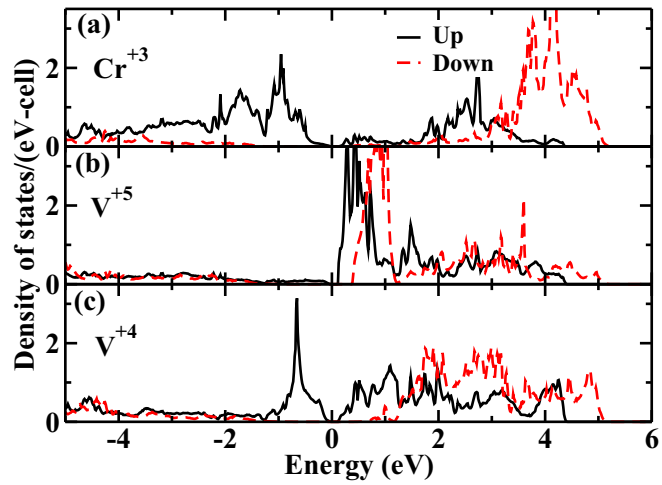



FIG. 3. Calculated spin projected transition metal *d* density of states for ferromagnetic Cr doped in rutile $VO_2$ at 12.5% doping (24-atom supercell). Different panels correspond to the atoms identified as (a) $Cr^{+3}$, (b) $V^{+5}$, and (c) $V^{+4}$ in the calculations.

TABLE II. Comparison of stability of ferromagnetic ground state and the next competing ground state AFM1 at 12.5% doping in the 24-atom supercell with variation of $U$ on Cr/V $d$ states. The relative energies as well as the magnetic moment (Mom) and band gap have been given.

| | $U$ (Cr, V) = 4, 3 eV | | | $U$ (Cr, V) = 5, 4 eV | | |
|---|---|---|---|---|---|---|
| | Energy (eV) | Mom ($\mu_B$) | Gap (eV) | Energy (eV) | Mom ($\mu_B$) | Gap (eV) |
| FM | 0.0 | 9.0 | 0.377 | 0.0 | 9.0 | 0.795 |
| AFM1 | 0.081 | 1.0 | 0.413 | 0.064 | 1.0 | 0.876 |

V atom. Examining the density of states associated with the other V atoms, we find that one can associate a valence of +4 with them.

The transition-metal–oxygen bond lengths better reflect the oxidation state when we use bond-valence concepts. The Cr-O bond lengths in the optimized structure were found to be 1.96 Å (×2) and 2.02 Å (×4). The presence of the longer bond lengths reflects the fact that the Cr atom has more electrons, and so minimizes the Coulomb repulsion between the electrons on Cr and those on O. All the V-O bond lengths were 1.96 Å in undoped $VO_2$. The $V^{+4}$-O bond lengths remain more or less similar to the parent compound with two bonds a little shorter (1.92/1.93 Å). As one would expect shorter V-O bond lengths for a higher valency of V atom, we also found the $V^{+5}$-O bond lengths to be 1.90 Å (×6), smaller than that of the $V^{+4}$-O ones. The $V^{4+}$ and $V^{5+}$ states correspond to a formal $d^1$ and $d^0$ configuration at the V site. As the number of electrons is higher at the V site for the $V^{4+}$ site, here, the V-O oxygen bonds have to be longer than between $V^{5+}$ atoms and oxygen. This leads to larger hopping interaction strengths in the latter case as against the former. Additionally the electrons in the higher valence state feel a stronger attraction from the nuclear potential. This leads to the $d$ levels being stabilized more, and consequently a smaller charge transfer energy for the higher valence V atom. Both of these factors contribute to stronger interactions between the V and the oxygen sites. Hence in this strongly hybridized picture, one ends up with very small differences in the number of electrons between the different valence states. With a small charge transfer energy as found here, one could also have a higher electron count for $V^{5+}$ than for the $V^{4+}$ atom [39]. The integrated transition metal $d$ component of the charge within spheres of radii 1.33 Å for Cr and 1.323 Å for V atoms on the sites labeled $V^{+4}$, $V^{+5}$, and $Cr^{+3}$ are found to be 3.35, 3.38, and 4.16. While a formal electron count of 1, 0, and 3 are expected in the transition metal $d$ orbitals based on the oxidation state, one finds the charge to deviate significantly from these values. The difficulty in partitioning charge in charge-ordered systems has been discussed in the literature [39–42] and we repeat the discussion for completion. The magnetic moments on the other hand are found to be 1.15, 0.21, 2.95 $\mu_B$. They reflect the valence state better as has been seen earlier [40]. However, here we find that the moment on $V^{+4}$ is higher than the value of 1 expected for the $d^1$ configuration that we have at the V site. This happens because the bare charge transfer energy is small and is equal to 0.5 eV and becomes negative when we include the bandwidth of the O $p$ states. This leads to the enhanced magnetic moment for $V^{+4}$ and $V^{+5}$ ions, over what is expected from a formal $d^1$ and $d^0$ configuration at the V sites.

The presence of charge ordering as well as the emergence of a ferromagnetic insulating state seems interesting, so we went on to examine whether these results were a consequence of the choice of $U$ on the V and Cr sites. As the literature [32–34] reports a range of values, we varied $U$ ($U_{Cr}/U_V$) from 3/2.5 eV to 5/4 eV. In every case we find the existence of $V^{+4}$, $V^{+5}$, and $Cr^{+3}$ ions. In order to examine the stability of the ferromagnetic insulating state, we again compute the energies for different magnetic ground states. The relative stability of the ferromagnetic insulating ground state compared to the competing antiferromagnetic AFM1 configuration as a function of $U$ is listed in Table II. In every case we find that the ferromagnetic state is stabilized and the conclusions remain unchanged. Hybrid functional calculations were also performed where the component of the Hartree-Fock exchange was chosen to be 25% as is usually considered for transition metal oxides. Here also we found a ferromagnetic insulating state to be stabilized by 0.094 eV over the closest lying antiferromagnetic state. The corresponding density of states plot is given in Fig. S2 of the Supplemental Material [36]. Magnetic moments on $Cr^{+3}$ and $V^{+4}/V^{+5}$ were found to be 2.91 and 1.12/0.16 $\mu_B$, respectively. The band gap was found to be 1.122 eV in contrast to the value of 0.1 eV we had for a $U$ of 3 eV on Cr and 2.5 eV on V, suggesting a larger value of $U$. We have not tried to determine the value of $U$ that would give us this band gap, as there is no consensus in the literature [43,44] on the appropriate value of the Hartree-Fock exchange for $VO_2$.

The choice of the supercell in the present instance has the $V^{+5}$ and $Cr^{+3}$ atoms arranged alternately in the $c$ direction along one of the chains. As this corresponds to a special configuration, we examined a larger unit cell of $\sqrt{2}\mathbf{a} \times \sqrt{2}\mathbf{b} \times 4\mathbf{c}$

TABLE III. Relative energies of different choices of FM and AFM1 configurations (columns 2 and 6) considered in a $\sqrt{(}2)\mathbf{a} \times \sqrt{(}2)\mathbf{b} \times 4\mathbf{c}$ supercell along with shortest distances between different pairs of Cr/V ions in columns 3, 4, and 5 are listed for the ferromagnetic configuration.

| | FM | | | | AFM1 |
|---|---|---|---|---|---|
| Configuration | Energy (eV) | $Cr^{+3}$-$Cr^{+3}$ (Å) | $Cr^{+3}$-$V^{+5}$ (Å) | $V^{+5}$-$V^{+5}$ (Å) | Energy (eV) |
| 1 | 0.0 | 4.450 | 3.433 | 4.450 | +0.204 |
| 2 | +0.155 | 5.902 | 2.962 3.461 | 5.403 | +0.400 |
| 3 | +0.019 | 3.486 | 2.962/3.461 | 5.316 | +0.224 |
| 4 | +0.119 | 2.921 | 3.475 | 4.451 | +0.298 |
| 5 | +0.064 | 5.341 | 3.450 | 4.452 | +0.245 |
| 6 | +0.017 | 5.400 | 2.955/3.436 | 3.521 | +0.302 |

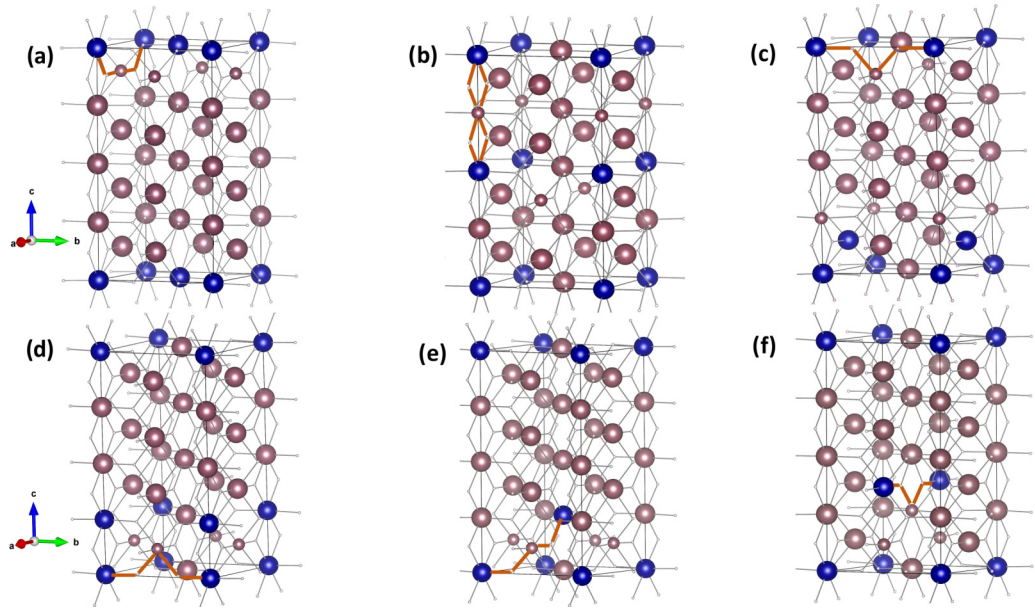



FIG. 4. Different choices considered for ferromagnetic arrangements of $Cr^{+3}$ (blue balls), $V^{+4}$ (big dark maroon balls), and $V^{+5}$ (small dark maroon balls) in $\sqrt{(2)}\mathbf{a} \times \sqrt{(2)}\mathbf{b} \times 4\mathbf{c}$ supercell of 12.5% Cr doped case. Small gray balls connecting these atoms are oxygen atoms. One of the Cr-$V^{5+}$-Cr pathways is highlighted by thick saffron lines in each of these figures.

which has 16 V atoms. We replaced two of the V atoms with Cr and explored all unique pairs possible within this unit cell. Relative energies with respect to the lowest ferromagnetic arrangement among various arrangement of doped Cr atoms in several ferromagnetic and possible AFM1 configurations are given in Table III. We have also tabulated the shortest distance between the $Cr^{+3}$-$Cr^{+3}$, $Cr^{+3}$-$V^{+5}$, and $V^{+5}$-$V^{+5}$ pairs in the ferromagnetic case. In six out of the seven arrangements of doped Cr atoms shown in Fig. 4, we have the ferromagnetic insulating state having lower energy. A continuous $V^{+5}$-$Cr^{+3}$ path is not necessary, but the presence of a pathway between two Cr atoms involving one $V^{+5}$ atom is found to stabilize the ferromagnetic insulating state. However, when the Cr atoms are far separated as in the seventh configuration, there is no such pathway possible. As a result, the ferromagnetic configuration is not favored. Having established the nature of the ground state, we revert back to the smaller unit cell for further analysis to understand the microscopic considerations that determine this unusual ground state.

We have calculated the *ab initio* band structure along various symmetry directions for a 24-atom unit cell of $VO_2$ in which one V atom is replaced by a Cr atom corresponding to a doping of 12.5%. No relaxation of the internal coordinates was carried out. A ferromagnetic configuration is assumed and a mapping onto a tight binding model was carried out for a model which had the transition metal $d$ and oxygen $p$ states in the basis. Here, the radial parts of the wave functions are considered to be maximally localized Wannier functions. The on-site energies were extracted from the above mapping. Based upon this analysis, an energy level diagram showing the position of various orbitals in the majority spin channel is shown in Fig. 5. Here we found that the lowest lying V-$d$ $t_{2g}$ orbital with the on-site energy 3.35 eV was ∼0.35 eV higher in energy than the highest Cr-$d$ $t_{2g}$ level with the on-site energy ∼3.0 eV. This is the reason that the Cr $d$ levels have three electrons on them. This large stability for the $Cr^{+3}$ configuration emerges from the large Hund's stability associated with a half-filled $t_{2g}$ band. Allowing for an optimization of the structure, we find that the structural distortions aid this ordering at the $Cr^{+3}$ site. Additionally, one finds that the oxygens around one V have distorted resulting in a $V^{+5}$ configuration. The other V atoms are in the +4

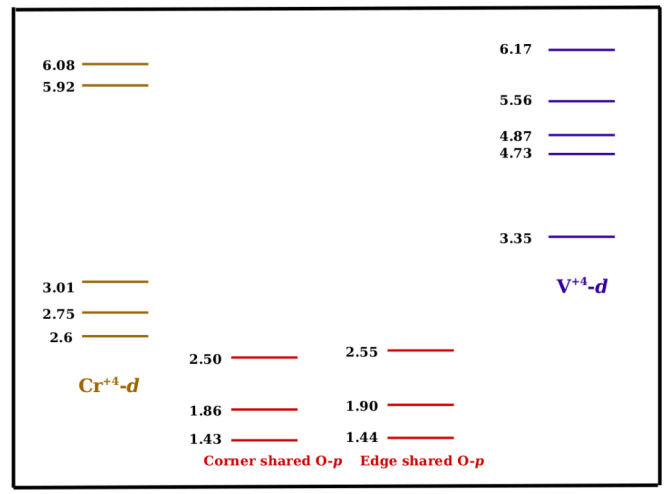



FIG. 5. Energy level diagram for $Cr^{+4}$ $d$ orbitals, corner and edge shared oxygen $p$ orbitals, and $V^{+4}$ $d$ orbitals in the unrelaxed ferromagnetic structure for 12.5% Cr doped $VO_2$. Energies (eV) for the majority spin channel have been given. This was obtained by fitting the *ab initio* band structure within a tight binding model considering Cr, V $d$, and O $p$ orbitals in the basis. The radial part of the tight binding basis functions are maximally localized Wannier functions.

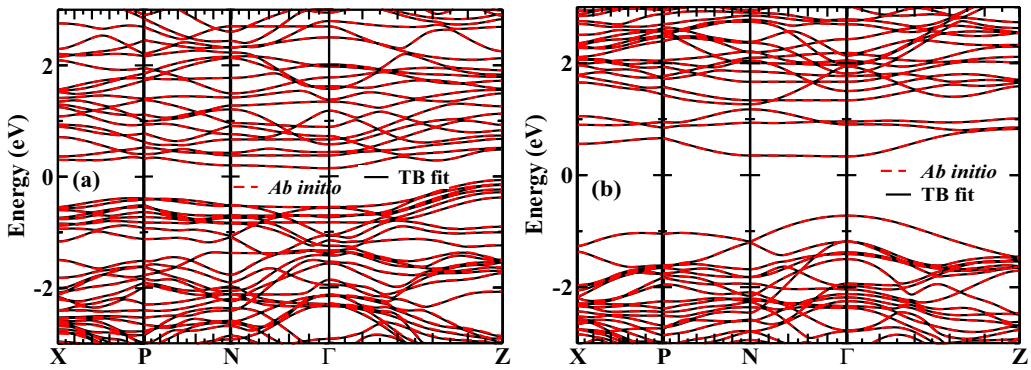



FIG. 6. A comparison of the *ab initio* spin-polarized band structure for ferromagnetic 12.5% Cr doped $VO_2$ for (a) up and (b) down spin channel and that obtained within a tight binding model considering Cr $d$, V $d$, and O $p$ states in the basis. Here, the radial part of the tight binding basis functions is maximally localized Wannier functions.

configuration and the system becomes insulating after the relaxations.

This analysis offers answers to a few of the questions raised earlier; however, a few questions remain unanswered, such as, why do we have a ferromagnetic ground state? Does the $Cr^{+3}$-$V^{+5}$ pair formation help in realizing a ferromagnetic state? In order to develop a clear understanding of these issues, we again carried out a mapping of the *ab initio* band structure for the ferromagnetic as well as the lowest lying antiferromagnetic state onto a tight binding model at the same doping concentration. A comparison of the spin-polarized *ab initio* band structure with the tight binding one in both the spin channels is shown in Fig. 6. One finds that one has a reasonably good description of the band structure which gives us the confidence to use the Hamiltonian for further analysis.

An estimate of the energy gain obtained from various hopping pathways available in this doped system would enable us to quantify their role in stabilization of such an unusual ground state. For this purpose, we artificially switch off the $Cr^{+3}$-$V^{+5}$ interactions via the intermediate oxygen atoms and calculated the band energy. A comparison of the evaluated band energy with the value obtained without switching off any interactions would provide us with the energy gain via the mentioned hopping pathways. This was done for both the ferromagnetic configuration as well as AFM1 which was the lowest lying antiferromagnetic configuration. We found that the gain in energy via this hopping channel in the ferromagnetic configuration was $\sim$7 eV per hopping pathway. However, when a similar analysis was done after switching off direct interaction between $Cr^{+3}$-$V^{+5}$ pairs, we found a very small energy gain of 0.065 eV. Based on these two results one can conclude that there is no direct pathway between the $Cr^{+3}$-$V^{+5}$ pair. The exchange pathway is through the oxygen atoms. We also estimated the energy gain from all $Cr^{+3}$-$V^{+4}$ hopping pathways via the oxygen atoms. We found the gain for the ferromagnetic configuration to be 3.11 eV per hopping pathway. We then did the same analysis for the next competing AFM1 configuration to present a comparative analysis in these two cases. The band energy gain in the AFM1 configuration from the most dominating channel of $Cr^{+3}$-$V^{+5}$ pairs via the oxygen atoms was found to be 6.293 eV per hopping pathway. It can hence be clearly seen that this gain is 0.7 eV larger in the case of the ferromagnetic configuration when compared to AFM1 configuration. This helps in stabilization of the ferromagnetic ground state. Contributions from direct interaction between $Cr^{+3}$-$V^{+5}$ pairs and from all $Cr^{+3}$-$V^{+4}$ hopping pathways via the oxygen atoms in the case of AFM1 are 0.217 eV and and 2.131 eV per hopping pathway, respectively. Although the direct hopping between $Cr^{+3}$-$V^{+4}$ pairs is larger in the AFM1 case, it is still substantially smaller than the channel via the oxygen atoms. The $Cr^{3+}$-$V^{+5}$ hopping interactions are again smaller in the AFM1 case when compared to the FM case. The substantial gain from the exchange pathway between Cr-V sites suggests an important role played by the charge ordering in stabilizing a ferromagnetic insulating state. Similar ideas were discussed by some of us in the context of another ferromagnetic insulator $K_2Cr_8O_{16}$ [14] and the present analysis is able to quantify the role of various exchange pathways.

Previous *ab initio* study suggested a half-metallic ferromagnetic character of Cr-doped $VO_2$ in the rutile phase at 25% doping [45], while higher doping concentrations closer to the $CrO_2$ end were examined in other theoretical papers [46,47]. This study was done considering a 12-atom supercell where replacing one of the V with a Cr atom corresponds to 25% doping. In order to investigate the system at this doping concentration, we replace two equivalent positions of the eight V atoms in our 24-atom supercell which corresponds to the same doping concentration. We allowed for volume optimization of this structure considering various magnetic configurations. The results comparing the total energy and the shortest distance between the $Cr^{+3}$, $Cr^{+3}$-$V^{+5}$, and $V^{+5}$-$V^{+5}$ pairs in different arrangements of Cr atoms in different ferromagnetic as well as various antiferromagnetic configurations at 25% doping are given in Table S2 of the Supplemental Material [36]. In Fig. S3, we have shown the arrangement of $Cr^{+3}$ and $V^{+4}/V^{+5}$ ions in the lowest energy ferromagnetic FM3 structure along with all the other antiferromagnetic configurations considered. Similar to 12.5% case, we also find a ferromagnetic insulating ground state in this case with formation of $Cr^{+3}$-$V^{+5}$ pairs. Cr has a magnetic moment of 2.863 $\mu_B$ while the atoms identified as $V^{+4}/V^{+5}$ have magnetic moments 1.12/0.453 $\mu_B$ for the FM3 configuration. We could not compare our results of the 25% Cr doped case with experiments as no data are available at this doping concentration.

## IV. CONCLUSION

The ferromagnetic insulating state found in Cr-doped $VO_2$ in the doping range from 10% to 20% has been investigated at the concentration of 12.5% within *ab initio* electronic structure calculations coupled with microscopic modeling within a tight binding model. We are able to reproduce the ferromagnetic insulating ground state within our calculations. Its stability is explained from the emergence of $Cr^{+3}$-$V^{+5}$ pairs which are found to be strongly stabilized by attractive Coulomb interactions. The presence of unoccupied $t_{2g}$ levels at the V sites and occupied $t_{2g}$ levels at the $Cr^{+3}$ site leads to a superexchange pathway via the oxygens. This is found to strongly stabilize the ferromagnetic insulating state and its role is quantified.

## ACKNOWLEDGMENTS

P.M. thanks SERB under the grant SERB-POWER SPF/2021/000066 for support. A.K. and S.S. thank CSIR for a fellowship to carry out the research.

[1] A. V. Chumak, V. I. Vasyuchka, A. A. Serga, and B. Hillebrands, Nat. Phys. **11**, 453 (2015).
[2] A. A. Serga, A. V. Chumak, and B. Hillebrands, J. Phys. D **43**, 264002 (2010).
[3] B. Huang, G. Clark, E. Navarro-Moratalla, D. R. Klein, R. Cheng, K. L. Seyler, D. Zhong, E. Schmidgall, M. A. McGuire, D. H. Cobden, W. Yao, D. Xiao, P. Jarillo-Herrero, and X. Xu, Nature (London) **546**, 270 (2017).
[4] S. Tian, J.-F. Zhang, C. Li, T. Ying, S. Li, X. Zhang, K. Liu, and H. Lei, J. Am. Chem. Soc. **141**, 5326 (2019).
[5] Y. K. Wakabayashi, Y. Krockenberger, N. Tsujimoto, T. Boykin, S. Tsuneyuki, Y. Taniyasu, and H. Yamamoto, Nat. Commun. **10**, 535 (2019).
[6] C. Gong, L. Li, Z. Li, H. Ji, A. Stern, Y. Xia, T. Cao, W. Bao, C. Wang, Y. Wang, Z. Q. Qiu, R. J. Cava, S. G. Louie, J. Xia, and X. Zhang, Nature (London) **546**, 265 (2017).
[7] J. Hemberger, P. Lunkenheimer, R. Fichtl, H.-A. Krug von Nidda, V. Tsurkan, and A. Loidl, Nature (London) **434**, 364 (2005).
[8] M. Azuma, K. Takata, T. Saito, S. Ishiwata, Y. Shimakawa, and M. Takano, J. Am. Chem. Soc. **127**, 8889 (2005).
[9] H. Das, U. V. Waghmare, T. Saha-Dasgupta, and D. D. Sarma, Phys. Rev. Lett. **100**, 186402 (2008).
[10] E. Pavarini, A. Yamasaki, J. Nuss, and O. K. Andersen, New J. Phys. **7**, 188 (2005).
[11] D. Meng, H. Guo, Z. Cui, C. Ma, J. Zhao, J. Lu, H. Xu, Z. Wang, X. Hu, Z. Fu, R. Peng, J. Guo, X. Zhai, G. J. Brown, R. Knize, and Y. Lu, Proc. Natl. Acad. Sci. USA **115**, 2873 (2018).
[12] P. A. Algarabel, J. M. De Teresa, J. Blasco, M. R. Ibarra, C. Kapusta, M. Sikora, D. Zajac, P. C. Riedi, and C. Ritter, Phys. Rev. B **67**, 134402 (2003).
[13] K. Hasegawa, M. Isobe, T. Yamauchi, H. Ueda, J.-I. Yamaura, H. Gotou, T. Yagi, H. Sato, and Y. Ueda, Phys. Rev. Lett. **103**, 146403 (2009).
[14] P. Mahadevan, A. Kumar, D. Choudhury, and D. D. Sarma, Phys. Rev. Lett. **104**, 256401 (2010).
[15] M. Marezio, D. B. McWhan, J. P. Remeika, and P. D. Dernier, Phys. Rev. B **5**, 2541 (1972).
[16] J. B. Goodenough and H. Y.-P. Hong, Phys. Rev. B **8**, 1323 (1973).
[17] J. P. Pouget, H. Launois, J. P. D'Haenens, P. Merenda, and T. M. Rice, Phys. Rev. Lett. **35**, 873 (1975).
[18] K. G. West, J. Lu, L. He, D. Kirkwood, W. Chen, T. P. Adl, M. S. Osofsky, S. B. Qadri, R. Hull, and S. A. Wolf, J. Supercond. Novel Magn. **21**, 87 (2008).
[19] L. F. J. Piper, A. DeMasi, S. W. Cho, A. R. H. Preston, J. Laverock, K. E. Smith, K. G. West, J. W. Lu, and S. A. Wolf, Phys. Rev. B **82**, 235103 (2010).
[20] Z. Yang, C. Ko, and S. Ramanathan, Annu. Rev. Mater. Res. **41**, 337 (2011).
[21] F. J. Morin, Phys. Rev. Lett. **3**, 34 (1959).
[22] M. W. Haverkort, Z. Hu, A. Tanaka, W. Reichelt, S. V. Streltsov, M. A. Korotin, V. I. Anisimov, H. H. Hsieh, H.-J. Lin, C. T. Chen, D. I. Khomskii, and L. H. Tjeng, Phys. Rev. Lett. **95**, 196404 (2005).
[23] T. C. Koethe, Z. Hu, M. W. Haverkort, C. Schüßler-Langeheine, F. Venturini, N. B. Brookes, O. Tjernberg, W. Reichelt, H. H. Hsieh, H.-J. Lin, C. T. Chen, and L. H. Tjeng, Phys. Rev. Lett. **97**, 116402 (2006).
[24] R. J. Soulen, J. M. Byers, M. S. Osofsky, B. Nadgorny, T. Ambrose, S. F. Cheng, P. R. Broussard, C. T. Tanaka, J. Nowak, J. S. Moodera, A. Barry, and J. M. D. Coey, Science **282**, 85 (1998).
[25] B. L. Chamberland, Crit. Rev. Solid State Mater. Sci. **7**, 1 (1977).
[26] Y. S. Dedkov, A. S. Vinogradov, M. Fonin, C. König, D. V. Vyalikh, A. B. Preobrajenski, S. A. Krasnikov, E. Y. Kleimenov, M. A. Nesterov, U. Rüdiger, S. L. Molodtsov, and G. Güntherodt, Phys. Rev. B **72**, 060401(R) (2005).
[27] J. M. D. Coey, A. E. Berkowitz, L. Balcells, F. F. Putris, and A. Barry, Phys. Rev. Lett. **80**, 3815 (1998).
[28] G. Kresse and J. Furthmüller, Comput. Mater. Sci. **6**, 15 (1996).
[29] G. Kresse and D. Joubert, Phys. Rev. B **59**, 1758 (1999).
[30] J. P. Perdew, K. Burke, and M. Ernzerhof, Phys. Rev. Lett. **77**, 3865 (1996).
[31] S. L. Dudarev, G. A. Botton, S. Y. Savrasov, C. J. Humphreys, and A. P. Sutton, Phys. Rev. B **57**, 1505 (1998).
[32] S. Lutfalla, V. Shapovalov, and A. T. Bell, J. Chem. Theory Comput. **7**, 2218 (2011).
[33] J. D. Budai, J. Hong, M. E. Manley, E. D. Specht, C. W. Li, J. Z. Tischler, D. L. Abernathy, A. H. Said, B. M. Leu, L. A. Boatner, R. J. McQueeney, and O. Delaire, Nature (London) **515**, 535 (2014).
[34] H. Lu, Y. Guo, and J. Robertson, Phys. Rev. Mater. **3**, 094603 (2019).
[35] D. B. McWhan, M. Marezio, J. P. Remeika, and P. D. Dernier, Phys. Rev. B **10**, 490 (1974).
[36] See Supplemental Material at http://link.aps.org/supplemental/10.1103/PhysRevB.104.125110 for additional details about optimized crystal structures, Wannier function spread, hybrid-functional based density of states plot, and magnetic con-

figurations and their corresponding energies for 25% doped case.

[37] A. A. Mostofi, J. R. Yates, Y.-S. Lee, I. Souza, D. Vanderbilt, and N. Marzari, Comput. Phys. Commun. **178**, 685 (2008).

[38] C. Franchini, R. Kováčik, M. Marsman, S. S. Murthy, J. He, C. Ederer, and G. Kresse, J. Phys.: Condens. Matter **24**, 235602 (2012).

[39] Y. Quan, V. Pardo, and W. E. Pickett, Phys. Rev. Lett. **109**, 216401 (2012).

[40] P. Mahadevan, K. Terakura, and D. D. Sarma, Phys. Rev. Lett. **87**, 066404 (2001).

[41] W. Luo, A. Franceschetti, M. Varela, J. Tao, S. J. Pennycook, and S. T. Pantelides, Phys. Rev. Lett. **99**, 036402 (2007).

[42] H. Raebiger, S. Lany, and A. Zunger, Nature (London) **453**, 763 (2008).

[43] R. Grau-Crespo, H. Wang, and U. Schwingenschlögl, Phys. Rev. B **86**, 081101(R) (2012).

[44] C. Franchini, J. Phys.: Condens. Matter **26**, 253202 (2014).

[45] M. E. Williams, W. H. Butler, C. K. Mewes, H. Sims, M. Chshiev, and S. K. Sarker, J. Appl. Phys. **105**, 07E510 (2009).

[46] M. E. Williams, H. Sims, D. Mazumdar, and W. H. Butler, Phys. Rev. B **86**, 235124 (2012).

[47] O. Mustonen, S. Vasala, T.-L. Chou, J.-M. Chen, and M. Karppinen, Phys. Rev. B **93**, 014405 (2016).